AUTOMATIC SEGMENTATION OF CONDUCTIVITY CHANGES IN ELECTRICAL IMPEDANCE TOMOGRAPHY IMAGES

A. Zifan, P. Liatsis, P. Kantartzis and R. Vargas-Canas
School of Engineering and Mathematical Sciences, City University, London, U.K.

Keywords: Electrical impedance tomography, Mesh, Probabilistic modeling and segmentation.

Abstract: In this paper, we propose a novel method for the automatic segmentation of Electrical Impedance Tomography (EIT) lung images. EIT is a non-invasive technique, which produces low-spatial and high-temporal resolution images of the internal resistivity of the region of the body probed by currents. EIT is the only technology that reliably quantifies regional lung volumes non-invasively. The problem is non-linear and ill-conditioned and can be solved using 2D or 3D finite element methods (FEMs) subject to using appropriate regularisation strategies. The usual method of segmenting EIT lung images is to manually select a region of interest and derive statistical measures. This procedure is not suitable for FEM-based models as it works on rectangular pixels, as well as making the task tedious and time consuming. We propose an alternative segmentation framework, which operates directly on the resulting FEM meshes, prior to rasterisation in order to prevent the propagation of errors in the reconstructed resistivity regions, due to mapping onto a rectangular grid. We use a spatio-temporal probabilistic method to segment conductivity changes in the EIT thorax images. Application of the proposed method offers a much needed alternative to interactive segmentation currently favoured by EIT researchers and clinicians.

1 INTRODUCTION

EIT is a non-invasive technique, which produces images of the internal conductivity or resistivity of the region of the body probed by alternating currents (Brown, 2003). EIT could be applied to imaging both structural and functional abnormalities in the human lungs. It has several advantages over existing chest-imaging techniques, including low cost, portability, its non-invasive and non-ionizing nature, the potential for ambulatory or ICU measurements and fast acquisition speed. EIT is the only non-invasive technique that provides insight into the regional distribution of ventilation. Current strategies to provide lung protective ventilation rely on avoiding lung over distension by reducing tidal volumes and on opening atelectasis by applying adequate positive end-expiratory pressure. However, it is currently impossible to continuously measure regional lung over distension and atelectasis while a patient is ventilated, but it would be extremely relevant information that could lead to reducing ventilator-induced lung injury. EIT can resolve changes in the distribution of lung volumes between dependent and non-dependent lung regions as ventilator parameters change. Thus, EIT measurements may be used to control the specific ventilator settings to maintain lung protective ventilation on an individual patient basis (Frerichs et al, 2006).

In EIT, current density flow within the body is described by Maxwell's equations. Typically, multiple electrodes are placed on a person's thorax and a sinusoidal current excitation is imposed. The governing equation for the voltage field produced by placing a current across a material is

$$\nabla \cdot (\sigma + \omega\varepsilon)\nabla\varphi = 0 \quad (1)$$

which is an elliptic partial differential equation, where σ is the electric impedance of the medium, φ is the electric potential, ω is the frequency, and ε is the electric permittivity (Molinari, 2003). Equation (1) is reduced to the standard governing equation for EIT, $\nabla \cdot (\sigma\nabla\varphi) = 0$ when the angular frequency is sufficiently low or direct current is used.

By repeating these steps and scanning around various electrode pairs, it is possible to calculate the approximate current distribution inside the body through inverse solution of Maxwell's equations using two or three-dimensional finite element

Zifan A., Liatsis P., Kantartzis P. and Vargas-Canas R..
AUTOMATIC SEGMENTATION OF CONDUCTIVITY CHANGES IN ELECTRICAL IMPEDANCE TOMOGRAPHY IMAGES.
DOI: 10.5220/0003157002150220
In *Proceedings of the International Conference on Bio-inspired Systems and Signal Processing* (BIOSIGNALS-2011), pages 215-220
ISBN: 978-989-8425-35-5

methods. A medical image can then be reconstructed, since the structures within the human body have different resistivities. However, this requires the solution of a non-linear, ill-conditioned inverse problem. The non-linearity arises in σ, since the potential distribution. φ, is a function of the impedance, φ= φ(σ), and the ill-conditioning stems from the fact that small errors in the measurements or in the forward modelling step may introduce large errors in the reconstruction. The forward problem in EIT is to estimate the induced electrical measurements at the electrodes, given an excitation signal and permittivity distribution. The inverse problem estimates the permittivity distribution based on the excitation signal and the terminal electrical measurements. Once images have been reconstructed, following regularization of the inverse problem, in the final stage, FEM triangulation results are rasterised to cover a rectangular grid for subsequent image processing.

2 EIT LUNG IMAGES

2.1 Low Spatial Resolution of EIT Images

It is well known that a reconstructed EIT image is unique for noise-free complete boundary data (Sylvester and Uhlmann, 1986). However, in comparison to magnetic resonance imaging (MRI) and computed tomography (CT), EIT suffers from poor spatial resolution due to noise, low sensitivity of boundary voltages to inner conductivity perturbations and a limited number of boundary voltage measurements (Clay and Ferree , 2002). Moreover, the reconstructed images are usually subtracted from a reference frame in order to minimize errors due to electrode movement or unknown boundary shape. A comparison of an EIT image and its CT counterpart of the thorax is shown in Figure 1. In spite of the above, EIT is very useful in monitoring patient lung volume, because the air has a large conductivity contrast compared to other tissues in the thorax. The large change in lung impedance with respiration, and the ease of use of impedance tomography as a monitoring technique, has led to a significant body of research in lung impedance (Frerichs, 2000). However, the spatial resolution of the EIT images reduces further with the rasterisation process, where FEM model results are mapped onto a rectangular grid for further image processing. This rasterisation step introduces further fuzziness to the reconstructed regions of conductivity changes in the EIT images of the lungs, and makes it even harder to determine the outline of these rapidly changing regions during the breathing cycle.

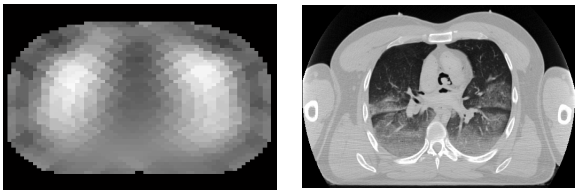

(a) (b)

Figure 1: (a) CT image of the thorax (Ackermann, 1995) (b) EIT difference image (brighter regions correspond to larger conductivity changes).

2.2 Feasibility of EIT Image Segmentation

Due to the aforementioned problems regarding the poor spatial resolution of EIT images, a question arises as to whether it is possible to introduce a robust adaptive EIT segmentation method. Currently, there exists no method, which could automatically segment regions with significant conductivity changes, corresponding to the lobes for an entire EIT breathing cycle sequence. The usual method of segmenting or interrogating images is to select a region of interest (a pixel or a small region) on the image and then derive statistical measures for the selected regions (Smallwood, 1999).

An additional problem is that EIT patient histories generally include data from a limited battery of tests, thus, making it difficult to train a sufficiently complete probabilistic model. Traditional background subtraction algorithms are not appropriate due to the slower inflation/ deflation rate of the lungs compared to the acquisition frame rate (i.e., 13 fps), hence changes in the lung lobe conductivity images appear slow moving or temporarily stationary. Under these conditions, the background becomes corrupted and object/blob detection becomes erroneous.

To address the above issues, in the following section a two-fold approach is proposed to tackle this. In the first step, we carry out segmentation on the FEM meshes prior to the rasterisation stage. This prevents regions becoming even fuzzier and facilitates the estimation of accurate measurement results, which is a prerequisite for the extraction of much needed ventilation parameters. In the second step, we use a probabilistic model, which accommodates both temporal and spatial contiguity of mesh element values in order to segment and

extract regions of conductivity changes directly from the EIT lung FEM meshes.

3 METHOD

3.1 Dealing with Non-rectangular Grids

The basis of the proposed approach is segmentation of conductivity changes on the actual FEM meshes, rather than the post-processed, rasterised images. This necessitates assigning a label to each triangular or tetrahedral element on the FEM mesh in order to access their coordinate positions. Unlike traditional images, which are typically based on rectangular grids, meshes can be of any shape and their constitutive elements maybe triangles in 2D or tetrahedra/ hexahedra in 3D. This restricts the applicability of image processing approaches, which are commonly implemented on rectangular grids. In the proposed method, we use the centroid of each triangular element composing the mesh (in our case, a 2D cross section of the thorax) as the representative of that particular element and we repeat this for all elements in the mesh. The coordinates of the centroids form the inputs for subsequent processing. A visual interpretation of the centroid concept on a sample mesh of the thorax obtained from EIDORS (Adler, 2006) is shown in Figure 2.

The next stage of the method consists of three steps. Firstly, we use anatomical information regarding the position of the lungs in the thorax to extract elements belonging to the background and obtain a prior model of the background by fitting a Gaussian to the trajectory of each background element value, E_{Bkg}, as it varies in time. Secondly, the change of mesh element values through time is modelled as an 'element process' and a Gaussian probability distribution is fitted to this trajectory, E_{ele}. Thirdly, an additional model, corresponding to the change of the sum of each element's neighbourhood associations through time, is formed by fitting a Gaussian probability model. The term 'neighbourhood association', denotes the connectivity neighbourhood value $E_{conn.}$ of mesh element $E(r,\theta)$, where (r,θ) are the polar coordinates of the elements' centroid, which consists of the number of adjacent triangles in the mesh that share a common edge with the current element. An example of neighbourhood association of the 251st element is shown in red patches in the mesh of Figure 2.

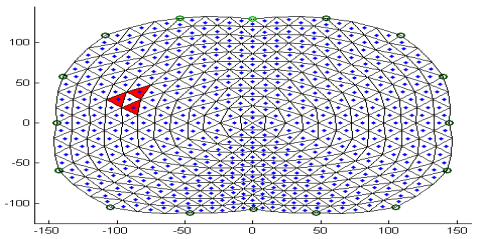

Figure 2: Centric assigned to each mesh element.

For this particular element the connectivity parameter will be

$$E_{conn} = \sum_{i=1}^{3} \left(E(r,\theta) - E(r_i,\theta_i) \right) \quad (2)$$

This parameter will be calculated for all elements in each frame in the sequence and a Gaussian model will be fitted to its trajectory. Finally, each new mesh element is classified by the closeness of its fit to the three Gaussian distributions (i.e., E_{Bkg}, E_{ele} and $E_{conn.}$).

3.2 Statistical Background Model

As previously discussed, the first task involves modeling of the background. This is achieved by using anatomical structure of the lung lobes. As observed in Figure 1(a), several layers exist between the lung lobes and the surface of the skin, i.e., skin tissue, fat layers, muscles covering the thorax and the thoracic skeleton, which protects the lungs.

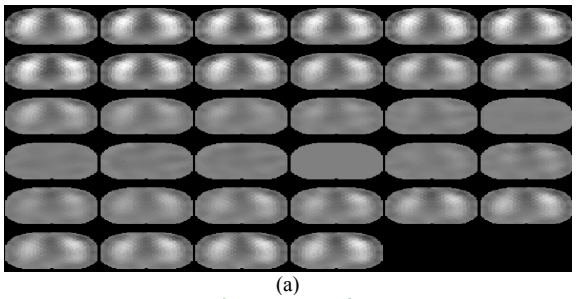

(a)

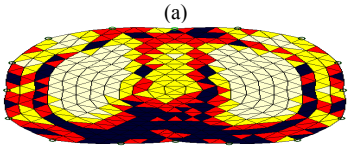

(b)

Figure 3: (a) Image progression is from left to right, top to bottom. Full-breath cycle is shown. (b) Variance mesh (Brighter regions correspond to higher conductivity variance).

This suggests that elements close to the boundary of the thorax do not form part of the lung lobes and thus background samples maybe extracted from these regions. In order to validate this hypothesis, we consider a sequence of reconstructed EIT FEM images corresponding to one of the patients in our dataset. The cycle is shown in Figure 3(a).

Next, we calculate the variance of each element over this period, and produce a variance image, as shown in Figure 3(b). As it is clearly seen, the lung lobes display the highest conductivity changes, followed by the adjacent darker region (depicted in red and black colours), which separates them from the other layers; we were able to reproduce such variance 'pattern' images for all patients in the dataset. Hence, the two most distant element layers from the mesh centre were used as background samples. For all of these elements in a frame sequence, we model their change trajectory as a random variable that follows a Gaussian distribution $p_{i,j} \sim \mathrm{N}(\mu_{i,j}, \sigma_{i,j}^2)$.

$$p_{i,j}(E_{i,j}(r,\theta)) = \frac{1}{\sigma_{i,j}\sqrt{2\pi}} e^{\frac{-(x-\mu_{i,j})^2}{2\sigma_{i,j}^2}} \quad (3)$$

where $p_{i,j}$ is a pixel-wise random variable which follows a Gaussian distribution, located at the j^{th} position in the i^{th} EIT frame sequence. (μ, σ) are the corresponding mean and standard deviation parameters of the Gaussian distribution. Hence, background mesh element values over time are modelled as a time series, which is called an element process.

Methods employing time-adaptive per-pixel mixture of Gaussians (MoG) are a popular choice for modelling scene backgrounds at the pixel level (Stauffer, 1999). In our application, one Gaussian sufficed, and moreover such methods are not appropriate for EIT, since we are not interested to merely segment out the foreground, but rather the lung lobes. This is better understood by examining Figure 3(b). It can be clearly seen that the current background model is not sufficient for lung lobe conductivity change segmentation. Specifically, the central region mesh elements also exhibit constant changes of conductivity; however, they do not belong to the lung lobes. For example, if we threshold the elements of this mesh using the 75 percent Quantile of the variance values we get the FEM shown in Figure 4.

As it can be seen in this figure, central regions also show a large degree of change in conductivity,

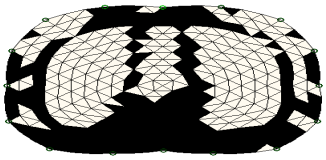

Figure 4: Thresholded variance image.

hence a Gaussian model fitted to the mesh element trajectories could indeed belong to the foreground; however, it may not necessarily form part of the lobes, which is the objective of this work. In order to resolve this problem, we build two further element process models, namely E_{ele} and $E_{conn.}$, the first representing changes of an individual element in time (excluding previous elements used for the background model) and the second representing the region attribute process in time, as discussed before. So, if the new element centroid was not classified as part of the initial background model, it would be part of the foreground but it may or not correspond to the lobe regions that we are after. Next, by comparing its value to our other two probabilities calculated for E_{ele} and $E_{conn.}$ we can then calculate whether it maximizes both these probabilities ensuring which only an element in the lobe region might do.

3.3 Element Classification

Each background element has its own threshold value, which can be obtained from the corresponding standard deviation. In this respect, the proposed method is similar to the adaptive method described in (Stauffer, 1999), i.e., a per-element/per-distribution thresholding method. The details of the algorithm are as follows:

1) Calculate Background model $N(\mu_{bg}, \sigma_{bg})$
2) For each element in current frame calculate $\mathrm{H}_{ie} = \left| E_i(r,\theta,t) - \mu_{ie} \right| \quad e = \{1,2\}$,
3) $\mathrm{T}_{ie} = \eta\sigma_{ie}$, $\mathrm{T}_{bg} = \eta\sigma_{bg}$
4) if $\mathrm{H}_{ie} < T_{bg}$ then element is background, update background. Go to Step 6 else it's a possible lobe
5) if $\mathrm{H}_{ie} > T_{bg}$ & $\mathrm{H}_{ie} > T_{ie}$ element belongs to the lung lobe region. Go to Step 2.
6) $\mu_{ie} = (1-\alpha)\mu_{ie} + \alpha E_i(r,\theta,t)$
   $\sigma_{ie} = (1-\alpha)\sigma_{ie} + \alpha E_i(r,\theta,t)$

Here, $E_i(r,\theta,t)$ is an element in a current frame (i^{th} in the sequence), μ_{i1} is the mean of the

element-wise Gaussian distribution, μ_{i2} is the mean for the regional attribute distribution, σ_{i1}, σ_{i2} are the corresponding element-wise standard deviations, respectively, H_{ie} is the absolute difference between E_i and the distribution means, T_{bg} and T_{ie} are the element-wise thresholds for E_{Bkg}, E_{ele} and $E_{conn.}$, α is the learning rate of the background and η is the threshold gain. $N(\mu_{bg}, \sigma_{bg})$ is pre-calculated and is not updated to accommodate for faster computation speed.

4 EXPERIMENTS AND RESULTS

4.1 Data Acquisition and Processing

Data were collected from a group of 10 male subjects with no known respiratory or cardiac abnormalities (age: mean 32; age range, 27-42). In each case, the 16 element adjacent electrodes were placed around the subject's lower thorax (4^{th}-6^{th} intercostal space on the mid-clavicular line). The subjects lay supine, and were asked to relax and breathe normally during a 3 min recording. A total of 2340 frames were recorded using a Sheffield mark 1 EIT system, using a 50 kHz current drive (Brown B. H. and Seagar A. D., 1987).

The measured voltage data were then imported into EIDORS and the inverse problem was solved using the Gauss-Newton reconstruction algorithm on a 2D, 576-element thorax mesh model, shown in Figure 2. The FEM triangulation results were not parameterized on a 2D pixel grid after the reconstruction, in order to prevent further resolution deterioration.

4.2 Gaussian Fitting and Element Classification

Next, the normalized element value trajectory alongside the regional attribute trajectory was fitted by two separate Gaussian models. More specifically, the recent history of each element, $\{E_{ele}(r,\theta,1),\ldots,E_{ele}(r,\theta,t)\}$ alongside the sum of its regional attributes $\{E_{conn}(r,\theta,1),\ldots,E_{conn}(r,\theta,t)\}$ were modelled by the two Gaussian distributions. The process of fitting the 251^{st} element of the mesh of figure 2, which is located in the upper left region of the mesh, is shown in Figure 5 for E_{ele}.

Finally, for each new frame, each of its elements

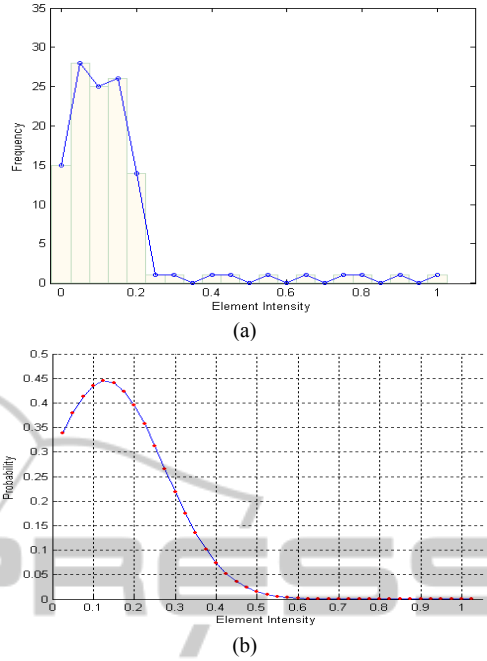

Figure 5: (a) Intensity histogram for the 251^{th} element in time (b) Fitted Gaussian probability distribution.

is classified to background or lung lobe region according to the algorithm described in section III. For the experiments, the learning rate parameter α was set to 0.002, while η = 2.5 gave the best classifications. The results of the proposed method on the EIT sequence of Figure 3(a) are shown in Figure 6.

The effectiveness of the proposed method can be seen from Figure 6. It shows that the probability models were able to separate out the non-lung lobe regions and picked out only areas of high conductivity changes produced by the lobes without producing outliers. With the proposed approach, the use of regional information of each element as it evolves through time permits the detection of the globality of the change, recovering the correct changes in the lobes.

5 CONCLUSIONS

The work proposes a novel, probabilistic method for extracting regions of conductivity changes in EIT lung images. The method involves modelling each mesh element and its regional attribute as a time series process fitted by a Gaussian model. Moreover, a prior model of the background was also obtained using anatomical structure of the thorax. The results obtained from the different patient data show that

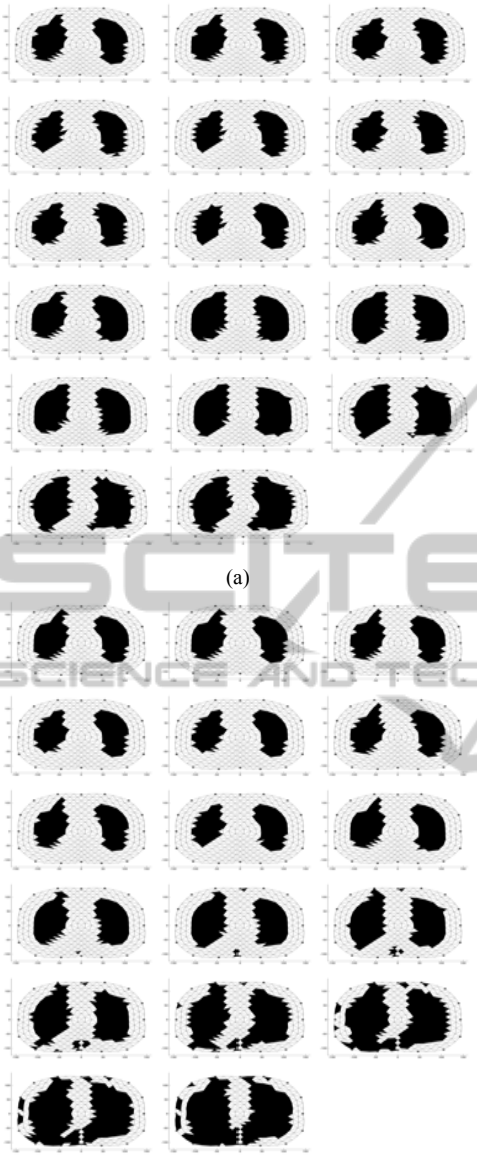

(a)

(b)

Figure 6: Segmentation results; image progression is from left to right, top to bottom. Full-breath cycle is shown. (a) proposed method (b) time-adaptive per-pixel MOG method described in (Stauffer, 1999).

this new approach can be successfully applied to automatically segment regions of conductivity changes in EIT lung images. The procedure requires minimal input fine-tuning and can capture the dynamics of distinctly different regions in EIT images. Further work involves the use of parallel processing to speed up the segmenta-ion process so that it can be used in real-time, for longer time periods, and the extension of the framework to segmentation on 3D meshes.

ACKNOWLEDGEMENTS

The authors gratefully acknowledge financial support of this research through the grant provided by the Engineering and Physical Sciences Research Council (EPSRC) under Grant EP/E029868/1.

REFERENCES

Ackermann M.J., 1995. The Visible Human Project. http://www.nlm.nih.gov, 1995. The authors gratefully acknowledge financial support of this research through the grant provided by the Engineering and Physical Sciences Research Council (EPSRC) under Grant EP/E029868/1.

Adler A. and Lionheart W. R. B., 2006. Uses and abuses of EIDORS: An extensible software base for EIT. *Physiol Meas,* 27:S25 {S42}

Brown B. H. and Seagar A. D., 1987. The Sheffield data collection system, *Clin. Phys. Physiol. Meas., 8*, (Suppl A) 91{97}.

Brown, B.H., 2003. Electrical impedance tomography (EIT): a review, *J Med Eng Technol.* vol.:27, pp.97-108.

Clay M.T. and Ferree T.C., 2002. Weighted regularization in electrical impedance tomography with applications to acute cerebral stroke. *IEEE Trans. Med. Imaging, Vol.* 21, pp.629–37.

Frerichs I., 2000. Electrical impedance tomography (EIT) in applications related to lung and ventilation: a review of experimental and clinical activities. *Physiological Measurement*, Vol. 21, no. 2, p. R1.

Frerichs, I., Scholz, J., and Weiler, N., 2006. Electrical Impedance Tomography and its Perspectives in Intensive Care Medicine. In J.L. Vincent (Ed.), *Yearbook of Intensive Care and Emergency Medicine, Berlin: Springer*, *vol.10, pp. 437-444,*

Molinari, M., 2003. High Fidelity Imaging in Electrical Impedance Tomography. Ph.D. thesis, University of Southampton, Southampton, United Kingdom.

Smallwood R. H., Hampshire A.R., Brown B.H., R. A., Primhak, Marven S. S., and Nopp P., 1999. A comparison of neonatal and adult lung impedances derived from EIT images. *Physiological Measurement*, Vol. 20, pp. 401-413.

Stauffer M. C., and W. Grimson, 1999. Adaptive background mixture models for real-time tracking. *IEEE Computer Society Conference on Computer Vision and Pattern Recognition (Cat. No PR00149). IEEE Comput. Soc. Part Vol. 2.*

Sylvester J. and G. Uhlmann, G., 1986. A uniqueness theory for an inverse boundary value problem in electrical prospection. *Commun. Pure Appl. Math., Vol.*39, pp.91–112.